JOURNAL OF SOLID STATE CHEMISTRY 120, 151–156 (1995)

# Raman Scattering and XAFS Study of Optically Nonlinear Glasses of the $TiO_2$–$NaPO_3$–$Na_2B_4O_7$ System

T. Cardinal, E. Fargin, and G. Le Flem

*Laboratoire de Chimie du Solide (UPR 866I, CNRS), Université de Bordeaux I, 351 Cours de La Libération, 33405 Talence Cedex, France*

and

M. Couzi

*Laboratoire Spectroscopie Moléculaire et Cristalline (URA 124, CNRS), Université de Bordeaux I, 351 Cours de La Libération, 33405 Talence Cedex, France*

Received February 14, 1995; revised May 22, 1995; accepted July 13, 1995

**Raman scattering and X-ray absorption studies have been performed on nonlinear optical glasses with compositions $x$$TiO_2$, $y$$NaPO_3$, $z$$Na_2B_4O_7$ ($y/z$ = 0.95/0.05 and $x$ = 0 to 42.2% molar). A model is proposed to explain the progressive modifications of Raman and XAFS spectra with increasing $x$. Two different types of oxygenated sites for titanium have been identified, in which Ti is respectively six-fold and five-fold coordinated. The rate of five-fold coordinated Ti is increasing with $x$, and the formation of Ti–O–Ti–O–... chains with alternating short and long Ti–O distances have been evidenced for the highest concentrations of $TiO_2$.** © 1995 Academic Press, Inc.

## INTRODUCTION

In the context of a general study of glasses containing high hyperpolarizable entities, samples of the $TiO_2$–$NaPO_3$–$Na_2B_4O_7$ system have been investigated. $TiO_2$ as rutile crystal and $TiO_2$ containing phosphate and silicate glasses have already been proven to be highly nonlinear (1, 2). As a general rule, the nonlinear refractive indices of the $TiO_2$ containing glasses increase with the ratio of titanium oxide. On the other hand, for the same concentrations of titanium phosphate glasses prove to be relatively more efficient than silicate glasses (2). In order to increase the intensity of the nonlinear response, it was of interest to find a glass matrix with a composition close to the previously studied phosphate matrix but able to include higher concentrations of $TiO_2$ (2). As reported by J. F. Ducel *et al.*, the introduction of a small proportion of $Na_2B_4O_7$ (5%) into $NaPO_3$ induces a considerable increase in the glass recrystallization temperature (3). The choice of this borophosphate glass matrix actually allows one to introduce up to 42.2% of $TiO_2$ and accordingly to improve the resulting nonlinear optical response of the material (4).

According to Lines, rutile finds its high nonlinearity in the hyperpolarizability of the Ti–O bond (5). Therefore, the nature of local environments around titanium atoms in glasses must be precisely determined in order to make correlations between the observed titanium sites geometry and the measured nonlinear response (4, 5).

In this context, this paper reports parallel Raman and X-ray absorption spectra analysis of borophosphate glasses with compositions $(1 - x)$[0.95 $NaPO_3$, 0.05 $Na_2B_4O_7$], $x$$TiO_2$ for which $x$ varies from 0 to 42.2% molar.

## EXPERIMENTAL SECTION AND DATA ANALYSIS

The glasses were prepared according to a previously described procedure (4).

### *A. Raman Measurements*

The Raman spectra have been recorded on a Dilor Z24 triple monochromator instrument. The 514.5 nm emission line of a Spectra Physics Model 171 argon ion laser was used for excitation with incident power around 200 mW. Detection was made with a Hamamatsu cooled photomultiplier coupled with a photon counting system. The spectral resolution was about 2 to 3 $cm^{-1}$. The colorless glassy samples were cut in the shape of parallelipipeds of about $5 \times 5 \times 2$ $mm^3$ with carefully polished surfaces.

### *B. X-Ray Absorption Analysis*

*XANES and EXAFS measurements.* The glasses were conditioned as finely ground powder and each sample was weighed and uniformly dispersed between two X-ray transparent Kapton adhesive tapes. In each case the mass of glass powder had been previously computed to avoid saturation effects and to optimize the signal-to-noise ratio.



0022-4596/95 $12.00

The titanium K-edge EXAFS (extended X-ray absorption fine structure) and XANES (X-ray absorption near-edge structure) spectra were recorded at room temperature at LURE, the French synchrotron radiation facility, by using an EXAFS III spectrometer. The operating conditions in the storage ring DCI were the following: positrons at energies of 1.85 GeV and intensities of about 250 mA. The double crystals Si (311) monochromator was detuned to discard harmonics from the beam. The spectra of $Ba_2TiO_4$, $TiO_2$ anatase, and $K_2O$–$TiO_2$–$2SiO_2$ glass were recorded as references; the first for an energy calibration ensuring an experimental accuracy in energy better than 0.3 eV, and the last two for testing the consistency of phase and amplitude parameters implemented in EXAFS simulations.

*Data-analysis.* Near-edge spectra are processed by substracting a linear background computed by least-square fitting before the pre-edge region and normalized by using the beginning of EXAFS oscillations as a unit. Energy calibration is carried out by taking the well-defined first maximum of absorbance in the edge of $Ba_2TiO_4$ spectrum.

EXAFS modulations are analyzed by using standard methods (6, 7). The continuous absorption background is estimated by fitting the spectrum before the edge by a Victoreen function, while the main absorption beyond the edge is fitted with an iterative procedure. Normalization of the EXAFS signal is then achieved (7). A single-scattering theory permits the expression of the EXAFS signal as a sum of functions over all the shells around titanium. Each shell function depends on $k$ the wavenumber of the ejected photoelectron, $N$ the number of atoms in the shell, $R$ the distance from the absorbing titanium atom, $\sigma^2$ the Debye–Waller coefficient related to thermal and static disorder, $\lambda(k)$ the electron mean free path, and $f(k)$ and $\Phi(k)$ the amplitude and the phase functions for this shell. Structural information can then be extracted by simulations using this function. The tabulated amplitude and phase functions of Teo *et al.* are used (8). The edge energy $E_0$ (included in the $k$ definition) is allowed to vary for simulations in view of ensuring the transferability of these tabulated parameters to our materials. The electron mean free path is approximated by $\lambda(k) = k/\Gamma$, where $\Gamma$ is used as a fitting parameter, the remaining fitted parameters being $N$, $\sigma^2$, and $R$.

## RESULTS AND DISCUSSION

### A. Raman Spectra Analysis

The parallel (VV) polarized Raman spectra for the studied glasses of compositions $0 \leq x \leq 42.2$ are compared with the spectrum of the silicate glass of composition $K_2O$–$TiO_2$–$2SiO_2$ in which the titanium is located in a unique pyramidal oxygenated site (Fig. 1) (9). The spectrum of the glass matrix ($x = 0$) had been previously analyzed (10).

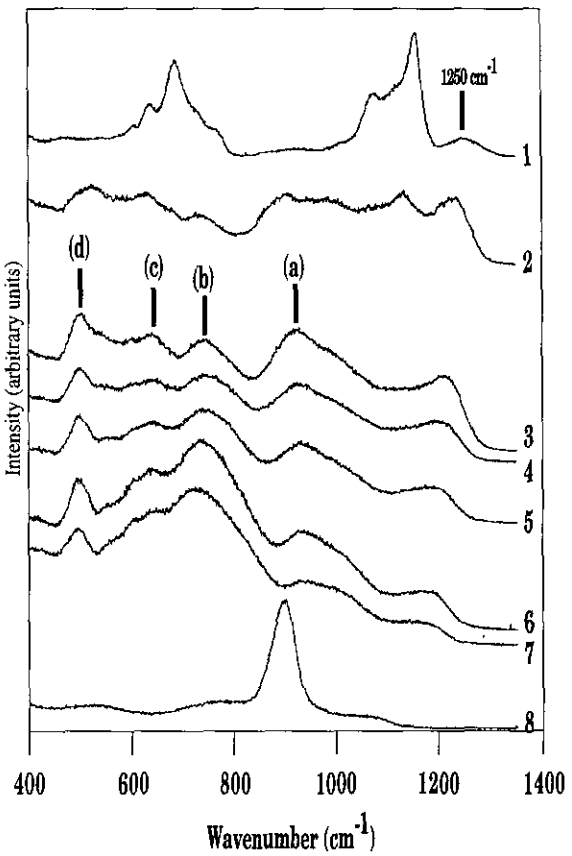


FIG. 1. Raman spectra of $x TiO_2$. $(1 - x)$[0.05 $Na_2B_4O_7$, 0.95 $NaPO_3$] glass samples of compositions $x = 0$ (1); $x = 15.0$ (2); $x = 26.3$ (3); $x = 29.0$ (4); $x = 33.3$ (5); $x = 38.5$ (6); $x = 42.2$ (7); and $K_2O$–$TiO_2$–$2SiO_2$ silicate glass (8).

The band observed at 1249 $cm^{-1}$ had been attributed to the $\nu$(P=O) vibration in P=O(–O–)$_3$ entities found in borophosphate groups, superimposed on the $\nu_{as}(PO_2)$ modes of metaphosphate units. The strong bands in the region of 1150 and 680 $cm^{-1}$ had been assigned, respectively, to the $\nu_s(PO_2)$ and the $\nu_s$(P–O–P) vibration modes of different metaphosphate units present in the borophosphate glass (10).

The progressive introduction of titanium oxide results in a disappearance of these phosphate bands except for that at 1249 $cm^{-1}$ which is continuously shifted to lower frequencies. Thus we conclude that the metaphosphate chains are broken and probably form titanophosphate units while preserving some of the nonbridging oxygen atoms and giving rise to a three-dimensional branching glass network.

The Ti–O vibrations are identified by four specific broad bands at around 930(a), 740(b), 640(c), and 500(d) $cm^{-1}$. The bands (a) and (b) exhibit a continuous evolution with increasing contents of $TiO_2$, the intensity of (a) decreasing progressively when compared to the intensity of (b). The

peak position of (a) is close to that of the strong band observed in the spectrum of the potassium silicate glass and can be unambiguously assigned to the $\nu$(Ti–O*) vibration where O* denotes an apical oxygen in a square based pyramidal environment of titanium (9, 11). The (b) band which is absent in the potassium silicate glass appears in the same frequency range as that of the intense bands previously observed in the spectra of $KTiOPO_4$ (KTP) and $NaTiOPO_4$ crystals (12, 13). This has been reported to prove the presence of –Ti—O–Ti—O–Ti— chains where short Ti–O bonds engage themselves and alternate with long Ti–O bonds (13, 14). The formation of such chains is obviously correlated to the vanishing of short Ti–O* free bonds responsible for peak (a).

Finally, the additional (c) and (d) bands could be the signature of distorted $TiO_6$ octahedra by referring to the previous analysis of $BaTiO_3$ and $K_2NiF_4$ type titanates spectra (15, 16). As a matter of fact, this assumption will be further reinforced by XAFS analysis.

### B. XANES Analysis

The near-edge spectra give qualitative information on the titanium environment. In particular, the pre-edge peaks are due to transitions of the photoelectron toward mixed $4p$(Ti), $3d$(Ti), and $2p$(O) vacant states and are then quite sensitive to the crystal field around titanium (17, 18, 19). Ti K-edge XANES spectra of our glasses for $x$ = 26.3, 33.3, 42.2, $TiO_2$ anatase, $K_2O$–$TiO_2$–$2SiO_2$ glass, and $Ba_2TiO_4$ are presented in Fig. 2. Details of the near-edge data are collected in Table 1. (Such close peak positions can unambiguously be compared to each other since the energy differences between different Ti sites symmetry features remain beyond experimental error.) $TiO_2$ anatase, $Ba_2TiO_4$, and $K_2O$–$TiO_2$–$2SiO_2$ glass can be considered as references for octahedral, tetrahedral, and square-based pyramidal geometries, respectively. The local structure of the previous silicate glass has effectively been proven without any ambiguity by simultaneous neutron scattering and EXAFS analysis (9). Each borophosphate glass spectrum exhibits a single pre-edge peak with shoulders on each side. Actually, this peak is the signature of the lack of an inversion center in the titanium sites and its energy is characteristic of square-based pyramidal sites, considering experimental accuracy in energy (Table 1). Its intensity slightly increases from 0.20 ($x$ = 26.3 %) to 0.27 ($x$ = 42.2 %). By a proportionality process using the height of the corresponding peak from the silicate reference glass, we can roughly deduce the rate of this type of site in borophosphate glasses. The resulting mean numbers of oxygen neighbors around titanium are summarized in Table 2. By contrast, the other features are characteristic of an octahedral symmetry.

TABLE 1
**Pre-edge Peak Parameters for Borophosphate Glasses and Reference Compounds**

| Materials | Peak position (±0.3 eV) | Peak height (±0.02) |
|---|---|---|
| $Ba_2TiO_4$ | 4968.2 | 0.81 |
| $K_2O$–$TiO_2$–$2SiO_2$ glass | 4969.5 | 0.43 |
| $TiO_2$ anatase | 4967.5 | 0.11 |
| | 4970.7 | 0.20 |
| | 4972.8 | 0.19 |
| Borophosphate glasses: | | |
| 26.3% $TiO_2$ | 4969.8 | 0.20 |
| 33.3% $TiO_2$ | 4969.8 | 0.23 |
| 42.2% $TiO_2$ | 4969.8 | 0.27 |

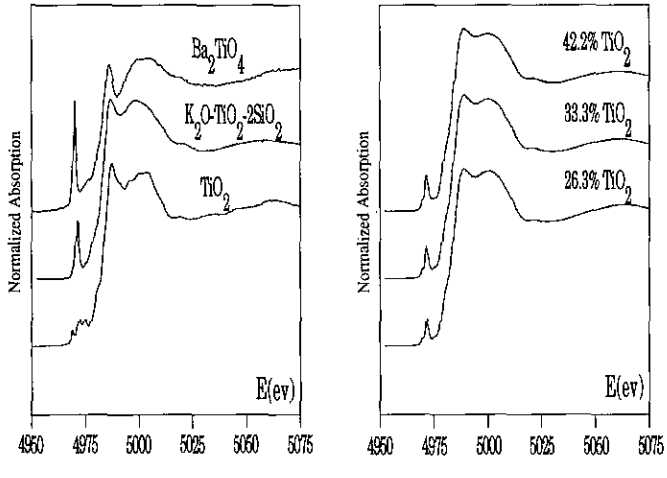


FIG. 2. Ti K-edge XANES spectra of borophosphates glasses and reference compounds.

### C. EXAFS Analysis

Fourier transforms of experimental EXAFS spectra ($\chi(k)$ in $k$ space), multiplied by $k^3$, are given in Fig. 3. These radial functions consist of $n$ peaks representing $n$ coordination shells at distances $R$ from Ti absorber without phase shift correction. On each Fourier transform, the first peak, which is the most intense, is due to the backscattering from the first neighboring oxygen atoms. Another small peak appears at larger distances, due to the backscattering of titanium atoms. Each peak corresponding to each shell is back-Fourier transformed and the resulting EXAFS signal is simulated using the previously described formalism. The results of fits are summarized in Table 2.

*Oxygen neighbors: first shell analysis.* The simulated spectra are represented on Fig. 4. Fitting attempts are first made with the references $TiO_2$ anatase and $K_2O$–$TiO_2$ $2SiO_2$ glass for testing the reliability of the Teo and Lee

TABLE 2
EXAFS Fit Results for the First Ti–O Shell

| Compounds | $N_1$ | $N_2$ | $R_1$ (Å) | $R_2$ (Å) | $\sigma^2(10^3$ Å$^2)$ | $E_0$ (eV) |
|---|---|---|---|---|---|---|
| $TiO_2$ anatase | 6.0 | | 1.93 | | 6.3 | 4998.1 |
| $K_2O$–$TiO_2$–$2SiO_2$ | 4.0 | 1.0 | 1.94 | 1.67 | 5.7 | 4998.5 |
| Borophosphate glasses: | | | | | | |
| 26.3% $TiO_2$ | 5.1 | 0.5 | 1.96 | 1.76 | 6.5 | 4997.2 |
| 33.3% $TiO_2$ | 5.0 | 0.5 | 1.97 | 1.69 | 7.2 | 4997.9 |
| 42.2% $TiO_2$ | 4.8 | 0.6 | 1.97 | 1.70 | 6.7 | 4997.8 |

*Note.* $R_1$ and $R_2$ are defined as two different Ti–O distances in the first oxygen shell around titanium atoms, $N_1$ and $N_2$ as the corresponding numbers of oxygen neighbors, and $\sigma^2$ and $E_0$ as the Debye–Waller factor and the threshold energy. For borophosphate glasses, $N_1$ and $N_2$ are deduced from XANES results with error bars estimated to 0.2 and 0.1, respectively.

amplitude and phase-shift parameters. In each case the number of oxygen neighbors was fixed (six for anatase, four in the plane square of pyramidal sites, and one in the axial direction for the silicate glass), and $E_0$, $\sigma^2$, $\Gamma$, and $R$ (two different distances for the silicate glass) were allowed to vary. In both cases the distances resulting from the best simulations indicate errors of about ±0.02 Å by comparison with published values (9, 20).

Then a fitting procedure is adopted for our series of glasses. A first parametrization is tested with only one distance, giving for each glass an $R$ value of about 1.96–1.98 Å and $N$ values between 5 and 6. But the corresponding simulated spectra $k\chi(k)$ have too long of a period for low $k$ values and too short of a period for large $k$ values. This is effectively observed when a few percentages of the neighbors are at a very short distance (6, 21). Actually, the introduction of an additional short distance (1.68 to 1.70 Å) in the fitting procedure is adopted. But, with the number of independent parameters for simulations being equal to 5, it has been necessary to drastically reduce the number of fitting parameters. First, the approximate numbers of oxygen neighbors which are deduced from XANES analysis are used. As can be seen in Tables 1 and 2, by considering the accuracy on the pre-edge peak height measures, the ratio of pyramidal sites can be taken as roughly constant and equal to about 50%. The numbers $N_1$ and $N_2$ of Ti–O bonds are then quite constant and equal to about 5 and 0.5 for the long and short distances, respectively. Then, if the same Teo and Lee amplitude and phase-shift parameters are used for both distances, the $E_0$, $\sigma^2$, and $\Gamma$ parameters would have to be different for each of these distances. Nevertheless, they are maintained identical for both distances $R_1$ and $R_2$ during the fitting procedures to assume the limitation of five independent fitting parameters. This can explain why the resulting simulations, especially for the $K_2O$–$TiO_2$–$2SiO_2$ glass reference, are not perfectly optimized (Fig. 4). Actually, the addition of a short Ti–O distance clearly improves the simulations. There is no significant evolution of $\sigma^2$, $\Gamma$, and $E_0$ in the final results for $x$ growing from 26.3 to 42.2% molar; their magnitude remains comparable to the corresponding parameters of the reference silicate glass and even $TiO_2$ anatase (Table 2).

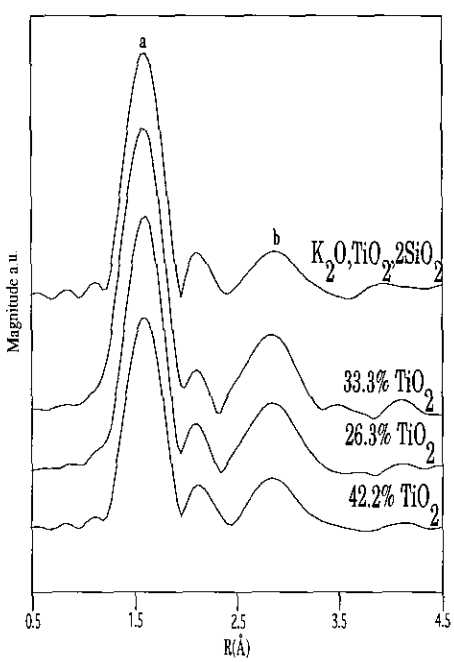


FIG. 3. Fourier transforms uncorrected for phase shift for three compositions of borophosphate glasses and the potassium silicate reference glass. a and b point to the first and second shell, respectively.

*Titanium neighbors: second shell analysis.* In the absence of an appropriate reference, the second shell has been filtered and fitted by using parameters from Teo *et al.* for all glasses including that of potassium silicate (8). There is evidence for the presence of Ti in this shell at a distance of 3.4 Å. It is unusual to observe an EXAFS signal for such a long distance in amorphous materials (large

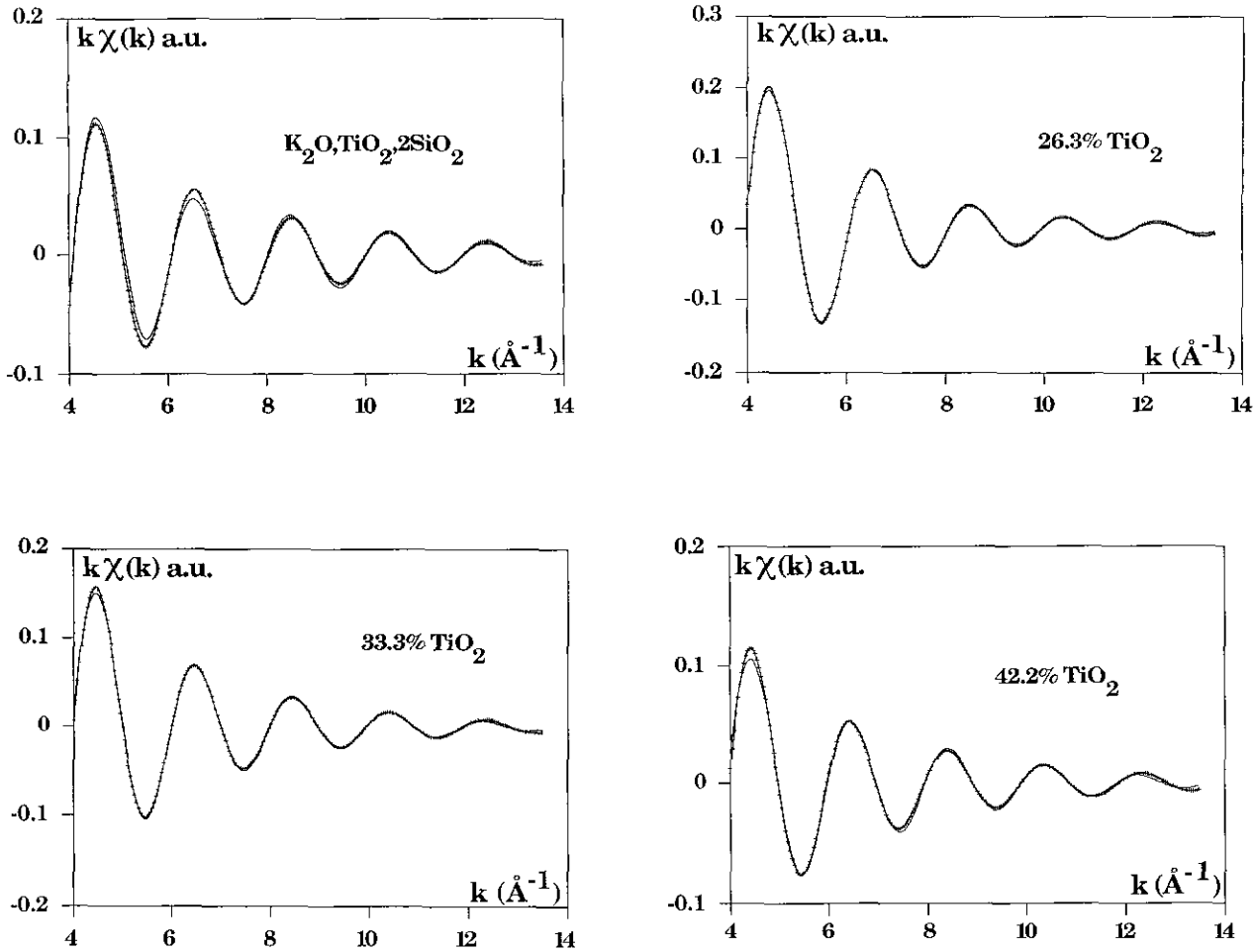


FIG. 4. EXAFS first shell signals (crossed lines) and least-squares simulations (solid lines) for three compositions of borophosphate glasses and the potassium silicate reference glass.

dispersion of distances). So it can be suggested that an enhancement of the signal could be produced by an intermediate oxygen atom into quasi-alignment with Ti atoms inducing the so-called focusing effect (6, 22). Then, in this case, the fitted values of $N$ and $\sigma^2$ cannot be reliable. Complementary neutron scattering experiments could probably give precise information on this second shell.

## CONCLUSION

The combination of Raman and XAFS spectra analysis allows one to identify the main structural features in borophosphate glasses where increasing proportions of $TiO_2$ are introduced.

First, the metaphosphate chains formed in the glass matrix are broken into titanophosphate groups.

Then, EXAFS analysis shows that the local environment of titanium atoms can be described by two different types of sites: either $TiO_5$ tetragonal pyramids with a short axial titanyl bond, or distorted $TiO_6$ octahedra. The octahedral coordination of $Ti^{4+}$ is usual in oxides, but the fivefold coordination has also been evidenced in several crystals such as $K_2Ti_2O_5$ (23). For this crystal the short distance is equal to 1.57 Å and the main peak in its Raman spectrum is observed at 905 $cm^{-1}$ (24). The presence of a similar band in the Raman spectra of borophosphate glasses is actually consistent with the formation of $TiO_5$ sites in these glasses.

Finally, EXAFS simulations of the second shell allow one to conclude that Ti–O–Ti–O ... chains are formed in both silicate and borophosphate glasses. Raman analysis gives further information showing that some chains alternating long and short Ti–O distances are spreading out with the concentration of $TiO_2$ in borophosphate glasses. This feature is observed in the KTP crystal, the structure of which consists of vertex-sharing $TiO_6$ octahedra cross-linked by phosphate groups to create a three-dimensional network (25). In contrast, the formation of such type of

chaining is not evidenced in the silicate glass by Raman analysis where branching can be described in this glass by interconnected corner-sharing $TiO_5$ pyramids and $SiO_4$ tetrahedra, as previously proposed by Yarker *et al.* (9).

To conclude, the original structural organization of $TiO_5$ sites in our borophosphate glasses could be responsible for the particularly high hyperpolarizability of the Ti–O bonds in the borophosphate glasses (4).

## ACKNOWLEDGMENT

We gratefully acknowledge LURE for provision of Synchrotron Radiation facilities.

## REFERENCES

1. E. M. Vogel, M. J. Weber, and D. M. Krol, *Phys. Chem. Glasses* **32,** 231 (1991).
2. C. Duchesne, *University Thesis,* Bordeaux, France, 1993.
3. J. F. Ducel and J. J. Videau, *Mater. Lett,* **13,** 271, (1992).
4. T. Cardinal, E. Fargin, G. Le Flem, L. Canioni, P. Segonds, L. Sarger, F. Adamietz, and A. Ducasse, *Eur. J. Solid State Inorg. Chem.* **31,** 935 (1994).
5. M. E. Lines, *Phys. Rev. B.* **43,** 11978 (1991).
6. B. K. Teo, "EXAFS: Basic Principles and Data Analysis." Springer–Verlag, Berlin, 1986.
7. We used the EXAFS data analysis set of programs written in Fortran 77 and implemented by A. Michalowicz (LURE 1985) on the Univac 1110 computer of Paris-Sud Informatique at Orsay. The programs are accessible and are available from A. Michalowicz.
8. B. K. Teo, P. A. Lee, A. L. Simons, P. Eisenberg, and B. M. Kinkaid, *J. Am. Chem. Soc.* **99,** 3854 (1977).
9. C. A. Yarker, P. A. V. Johnson, A. C. Wright, J. Wong, R. B. Greegor, F. W. Lytle, and R. N. Sinclair, *J. Non-Cryst. Solids* **79,** 117 (1986).
10. J. F. Ducel, J. J. Videau, and M. Couzi, *Phys. Chem. Glasses* **34,** 212 (1993).
11. S. A. Markgraf, S. K. V. Sharma, and A. S. Bhalla, *J. Am. Ceram. Soc.* **75,** 2630 (1992).
12. G. E. Kugel, F. Brehat, B. Wyncke, M. D. Fontana, G. Marnier, C. Caratabos-Nedelec, and J. Mangin, *J. Phys. C: Solid State Phys.* **21,** 5565 (1988).
13. C. E. Bamberger, G. M. Begun, and O. B. Cavin, *J. Solid State Chem.* **73,** 317 (1988).
14. J. C. Bailar, H. J. Emeleus, R. Nyholm, J. Wong, and A. F. Trotman-Dickenson, *in* "Comprehensive Inorganic Chemistry" (J. C. Bailar *et al.*, Eds.), **Vol. 3,** p. 317. Pergamon, Oxford, 1973.
15. G. Blasse and G. P. M. Van Den Huevel, *J. Solid State. Chem.* **10,** 206 (1974).
16. A. Bertoluzza, A. Marinangelli, M. A. Morelli, and R. Simoni, *J. Non-Cryst. Solids* **45,** 149 (1981).
17. J. Wong, F. W. Lytle, R. P. Messmer, and D. H. Maylotte, *Phys. Rev. B* **30,** 5596 (1984).
18. F. Babonneau, S. Doeuff, A. Leaustic, A. Sanchez, C. Cartier, and M. Verdaguer, *Inorg. Chem.* **27,** 3166 (1988).
19. F. W. Lytle, R. B. Greegor, and I. D. Raistrick, *J. Phys. C* **8–47,** 719 (1986).
20. M. Primet, P. Pichat, and M. V. Mathieu, *J. Phys. Chem.,* **75,** 1216 (1971).
21. E. Fargin, C. Duchesne, R. Olazcuaga, G. Le Flem, C. Cartier, P. Segonds, L. Canioni, L. Sarger, and A. Ducasse, *J. Non-Cryst. Solids* **168,** 132 (1994).
22. B. K. Teo, *in* "EXAFS Spectroscopy: Technique and Applications" (B. K. Teo and D. C. Joy, Eds.), p. 13. Plenum, New York, 1981.
23. S. Anderson and A. D. Wadsley, *Acta. Chem. Scand.* **15,** 663 (1961).
24. S. Sakka, F. Miyaji, and K. Fukumi, *J. Non-Cryst. Solids* **112,** 64 (1989).
25. I. Tordjman, R. Masse, and J. C. Guittel, *Z. Krystallogr.* **139,** 103 (1974).